UDC 539.4

Deformability Behavior of St3 Steel Used in the Profiles of High-Voltage Poles

A. Jutas,[a] J. Mockiene,[b,1] V. Vaiciukynas,[c] G. Zaldarys,[d] and G. Cinelis[b]

[a] Department of Mechanical Engineering, Faculty of Mechanical Engineering and Design, Kaunas University of Technology, Kaunas, Lithuania

[b] Department of Building Structures, Faculty of Civil Engineering and Architecture, Kaunas University of Technology, Kaunas, Lithuania

[c] Faculty of Water and Land Management, Aleksandras Stulginskis University, Kaunas District Municipality, Lithuania

[d] Department of Production Engineering, Faculty of Mechanical Engineering and Design, Kaunas University of Technology, Kaunas, Lithuania

[1] jurate.mockiene@ktu.lt

УДК 539.4

Характеристика деформованості сталі Ст3 для профілів високовольтних опор

А. Ютас[а], Ю. Моцкіене[б], В. Вайцюкинас[в], Г. Жалдарис[г], Г. Цінеліс[б]

[а] Кафедра машинобудування, Факультет машинобудування і проектування, Каунаський університет технології, Каунас, Литва

[б] Кафедра будівельних конструкцій, Факультет цивільного будівництва і архітектури, Каунаський університет технології, Каунас, Литва

[в] Факультет водокористування і землеустрою, Університет ім. Олександра Стулгінскіса, Районний муніципалітет м. Каунаса, Каунас, Литва

[г] Кафедра технології виробництва, Факультет машинобудування і проектування, Каунаський університет технології, Каунас, Литва

Установлено причини зміни механічних властивостей холоднокатаних кутиків із низьколегованої сталі Ст3 для старих конструкцій високовольтних опор. Вивчено ряд кінетичних кривих, що описують механічні властивості, у вигляді дотичних і пластичних модулів як найбільш прийнятних характеристик, оскільки узагальнені параметри можуть чіткіше відобразити зміну міцності і деформованості на будь якому етапі деформування. Представлено вихідні кількісні характеристики з метою виключення впливу якості елементів опор при їх виготовленні, щоб показати значення деформаційної поведінки для пояснення мікроструктурної різноманітності. Мікроструктурні характеристики можуть впливати на рівень напружень у точках плинності, границі міцності і руйнування.

Ключові слова: опора, сталь Ст3, корозія під напруженням, мікроструктура.

Introduction. This research was triggered by the initiative of mounting a new high-voltage electricity connecting different countries of Europe, including Scandinavia. During its installation, multiple electricity poles built no later than in 1956 have been dismounted but many old poles still remain in Lithuania and beyond its borders. High-voltage poles made in 1956 had to satisfy the cross-sectional geometry related standard (GOST 8509-57 confirmed later). Although the confirmed standard of St3 steel (GOST 380-71) had new requirements and clear criteria of microstructure acceptance, some

poles with a inhomogeneous microstructure remained in operation. In Lithuania, for its geographic situation the flows of polluted air (aggressive clouds) affecting high-rise buildings can come from various regions: during most seasons, they reach Lithuania from industrial regions brought by the South West and West winds and the closer Kaliningrad region. In the winter prevailing North East winds bring the contaminants from industrial regions of Belorussia and Russia and from some military objects [1]. Various winds and local atmospheric vortexes spread locally or coming to Lithuania from neighbor countries formed pollution products. According to this, an evaluation of the capacity of steel parts with localized corrosion is an important task for maintenance and retrofit activities [2]. In addition to those causes mentioned above, the elements may be affected by the others climate factors (precipitation, cold, wind, sun, dust, not proper covering of the anticorrosive material, etc), which are difficult to evaluate because of their random dissemination in the territory.

Corrosion depth and area, microstructural inhomogeneity of pole elements were evaluated in order to explain the reason of their influence on tensile mechanical properties. If degree of corrosion is the dominant factor, it may affect a capability to resist loads [3]. Some other researches have presented data on the structural behavior of corroded steel angles and the recommendations were drawn to provide guidance to engineers on how to evaluate compressive capacity of corroded elements. The differences in microstructure and corrosion related damages influence on the dissipation of mechanical properties. The structural capability to resist loads is related with the degrading effects on structural elements and quality of their microstructure gotten after a material manufacturing. Steel specimens contain microstructural defects with large amount of nonmetallic inclusions (iron oxides and sulfides), decarbonized surface layer, layered microstructure and the Widmanstätten structure. Nonmetallic inclusions were visible in all the specimens.

The potential of strength and deformability or toughness as the characteristic related to the quality of microstructure was expressed using so called relative deformation sensitivity parameter (RDSP). Despite the method simplicity described, RDSP may be one of the main criteria quantitatively characterizing any sets' differences classified according to a variety of microstructure, level of corrosion, thermal treatment and others.

Also as the most important experimental part of present investigation, the parameters of corrosion, mechanical properties and microstructural defects on speciments of St3 low-carbon steel were carried out by the micrometer, tensile testing machine and optical microscopy, respectively. The results have showed that the significant differences can be found in yield, ultimate and fracture stresses.

The present investigation was related to the fact that the uniform chemical composition and fine microstructure of material St3 had not been technologically achieved in the examined specimens and, as expected, an influence of corrosion could be relatively low.

1. **Experimental Details**. The specimens for tensile test were prepared from the dismounted poles having purpose to check their mechanical properties because many poles' types of high voltage electricity are still being used. The standard GOST 1497-84 (European standard ISO 6892-84) was used for the specimens' preparation and experiment implementation. The specimens were cut from the pole angle made of St3 steel. Specimen's illustration is presented in Fig. 1a and its dimensions in Table 1.

Measurements of corrosion depth were made on both sides of specimens. The depth was measured using ICh 10 micrometer indicator which precision is 0.01 mm. The corrosion depths were measured on both sides of specimens. The measurements were performed (along the specimen) every 3 mm. The measurement scheme of corrosion depth is shown in Fig. 1b.

An Axio Scope A1 (Carl Zeiss) optical microscope was used to visualize the microstructure at fracture areas taken after the tensile test.

T a b l e 1

Specimen Dimensions

Specimens	Geometric parameters							
	L, mm	B, mm	l, mm	h, mm	n, mm	b, mm	a, mm	r, mm
$u_1 ... u_4$	290	40	150	50	20	19.5-20.6	5-6	30
$m_1 ... m_5$	290	40	150	50	20	19.5-20.6	7-7.3	30

Note: $u_1 ... u_4$ and $m_1 ... m_5$ are the upper and middle parts, respectively.

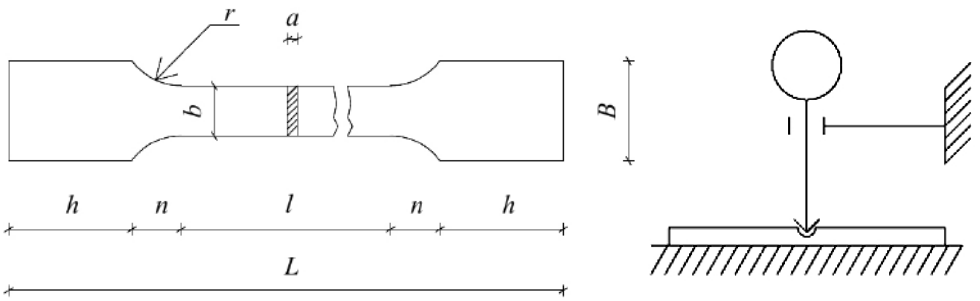

a b

Fig. 1. Scheme of specimen for tensile test (a) and measurement scheme of corrosion depth (b).

The specimens were affected by the external climatic factors (precipitation, cold, wind, sun, dust, etc.). The assumption can be done that one side of specimen can be damaged more than the other one because of more intensive action by above mentioned factors. For that reason the comparative analysis was performed that is to say both sides of specimens were explored if they were equally affected by corrosion processes. After the corrosion depths were measured the averages of collected data, standard errors of the average values, standard deviation, asymmetry coefficient, and other statistical parameters were calculated. The evaluation of data using the descriptive statistics was performed (Table 2). For data analysis, 763 measurements were used.

T a b l e 2

Main Parameters of Descriptive Statistics for Metal Damage Depth Analysis

Parameter	Statistics	Standard error
Average	0.094	0.0014
95% lower confidence average bound	0.091	
95% upper confidence average bound	0.097	
Average after eliminating 5% minimal and maximal values	0.093	
Standard deviation	0.039	
Maximal value	0.210	
Minimal value	0.010	
Difference between maximal and minimal values	0.200	
Asymmetry coefficient	0.237	0.089

It is obvious (Fig. 2) that corrosion damage depths in different specimens are not uniformly distributed. Performing the comparison of different sides of corrosion damages averages it was stated that practically there is no difference between the achieved values (0.094487–0.094498 mm). After the measurements of all specimens we found out the average of corrosion depth 0.094 mm. Taking into account the confidence interval with probability 95% we can see that interval of average value of damaged by corrosion specimen is in the range interval 0.091 and 0.097 mm. If we eliminate 5% of maximal and minimal values of damaged specimens we derive the average value that is very close to the calculated average – 0.097 mm. The measured corrosion values are different from average 0.039 mm. Maximal difference between the values is 0.2 mm. When rating the asymmetry coefficient one can state that the distribution curve is more stretched to the right side towards larger values measuring from the top of curve. Hence we can state that there are more values corresponding with more deeply penetrated corrosion. After the averages assessment of corrosion damage depth on both sides we stated that there was some relation between the depths on both sides but it is not strong. Taking into account the fact that the metal corrosion processes on both sides of specimens had had random character we examined if there was the relation between the depth of specimen corrosion and damage area of specimen. The corrosion area of explored specimens was calculated using Photoshop program. During calculation process the program automatically identified color intensity of corroded part and its area. Initially, the area was computed as defined in pixels, which afterwards were recounted into area units expressed in cm^2. Corrosion areas were calculated for eight specimens.

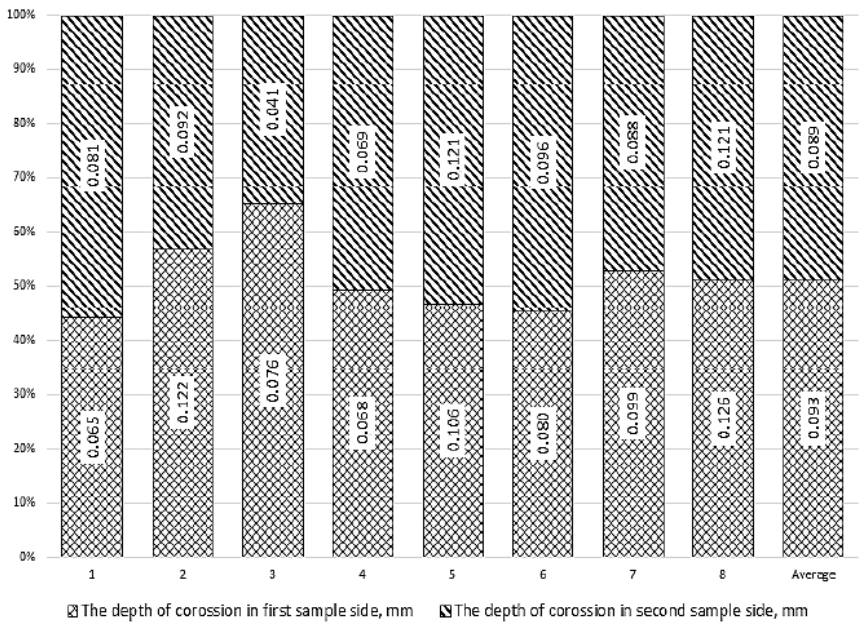

Fig. 2. Assessment of corrosion average depth values on different sides of the damaged specimens.

During the research it was found that the differences of corroded area in various specimens were in the range 0.26 to 3.06 cm^2 (Fig. 3). Investigation of the corrosion damage area of specimens determined that the corrosion area average is about 1.24 cm^2 or 31% of measured area. Maximal corrosion damage area was fixed in the specimen No. 2, the smallest corrosion damage area was found in the specimen No. 7. Also the damage area calculations showed that these areas are very different in size in separate specimens.

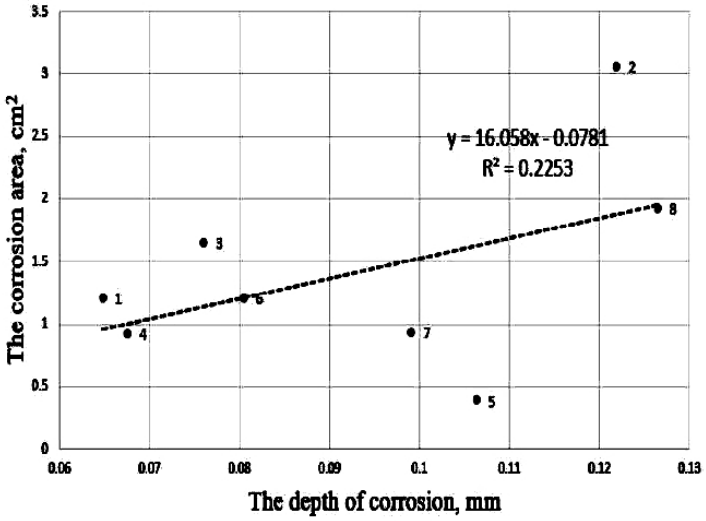

Fig. 3. Graphical relation of corrosion area and corrosion depth.

In this paper, two types of problems are solved using statistics methods: first, relation definition between the variables and second, relation strength definition between them. Relations between occurrences can be defined as reason and sequence, functional, statistical. Statistical relations exhibits only a reason and a sequence or functional relations, they mainly express more or less likely or probabilistic tendency represented as particular approximate compatibility of two variables values changed. The measurements showed that there was no relation between the damage depth and damage area among all the specimens. It could be explained assessing an inequality in chemical composition of metal when it was fabricating to be as a part of the electricity pole. It could be the reason of the extensive corrosion depths and areas. The climatic factors influencing on the poles and that also should be taken into account are: precipitation, air pollution, UV-rays, temperature changes. When the parts were covered by the anticorrosive materials, the human factor should be also be considered. It has been too complicated to evaluate all the above, that is why they are not assessed in this paper.

There were performed measurements of depths on both sides of specimens while seeking to evaluate the influence of corrosion depth to yield force. The values achieved were summed up because the corrosion has affected both sides of specimens.

Large values of damage depth may affect the metal strength. There was a hypothesis under consideration that the metal specimen thinning formed as a result of corrosion can influence on the metal tensile strength. The tensile experiment was provided to confirm or decline the corrosion depth influence on the material strength (Fig. 4).

The diagram illustrates the fact that the increase in corrosion depth almost does not affect maximal yield stress limits which remains in the range 280–350 MPa. Looking at the general tendency one can notice that the yield stress values increase slightly when the corrosion depth increases.

Similar results were achieved investigating the ultimate stress. Performed investigations showed that with the increment of corrosion depth the ultimate stress changes in not a large range 380 to 500 MPa (Fig. 4). As in the first case when the corrosion depth influence to yield stresses was investigated, the strength has slightly decrease tendency when the corrosion depth increases.

Erosion depth influence analysis to elongation per unit of specimen showed a similar tendency as that in previous two cases: when corrosion depth increases, the measured

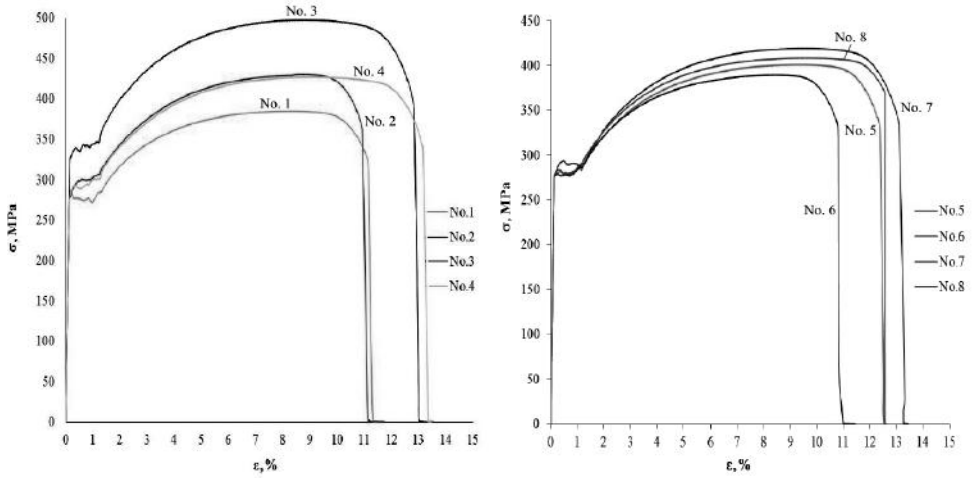

a b

Fig. 4. Tensile diagrams: (a) upper pole part (UPP); (b) middle pole part (MPP).

elongation per unit value changes in the narrow (11 to 13%) range (Fig. 4). However, reviewing the general tendency of the performed experiment it can be noticed that if the corrosion depth increases the specimen elongation per unit also increases.

Microstructural properties have allowed featuring of differences in mechanical properties that is why an analysis gains more comprehensive explanation. In this paper, the following features describing microstructural nature were used: 0 – homogeneity; A – inhomogeneity; B – nonmetallic inclusions; C – layered microstructure (residual ferrite bands); D – Widmantstätten; E – de-carbonization (see Fig. 5). Feature strength was determined using levels from I (the weakest) to V (the strongest) according to microstructural feature/defect amount (see Table 3). The upper part of the pole represents the material (specimens Nos. 1, 2, 3, and 4) with widely distributed values at the points of yielding and ultimate strength comparing ones with the middle part (specimens Nos. 5, 6, 7, and 8).

T a b l e 3

Microstructural Features (A–E) and Their Levels (I–V) at the Area of Fracture in Specimens Nos. 1–8

Specimen No.	Microstructural properties and levels					
	$C(C_1...C_n)$, %	A	B	C	D	E
1 (13)	0.15 (0.13...0.18)*	IV	V	IV	–	I
2 (15)	0.15 (0.13...0.18)	V	V	II	II	I
3 (18, 37)	0.15 (0.13...0.18)	I	I	III	–	I
4 (25)	0.15 (0.13...0.18)	II	II	I	–	I
5 (6)	0.25 (0.2...0.3)	IV	V	II	II	–
6 (8)	0.25 (0.2...0.3)*	III	V	II	I	–
7 (9)	0.25 (0.2...0.3)	II	I	II	–	–
8 (28)	0.25 (0.2...0.3)	IV	I	II	–	–

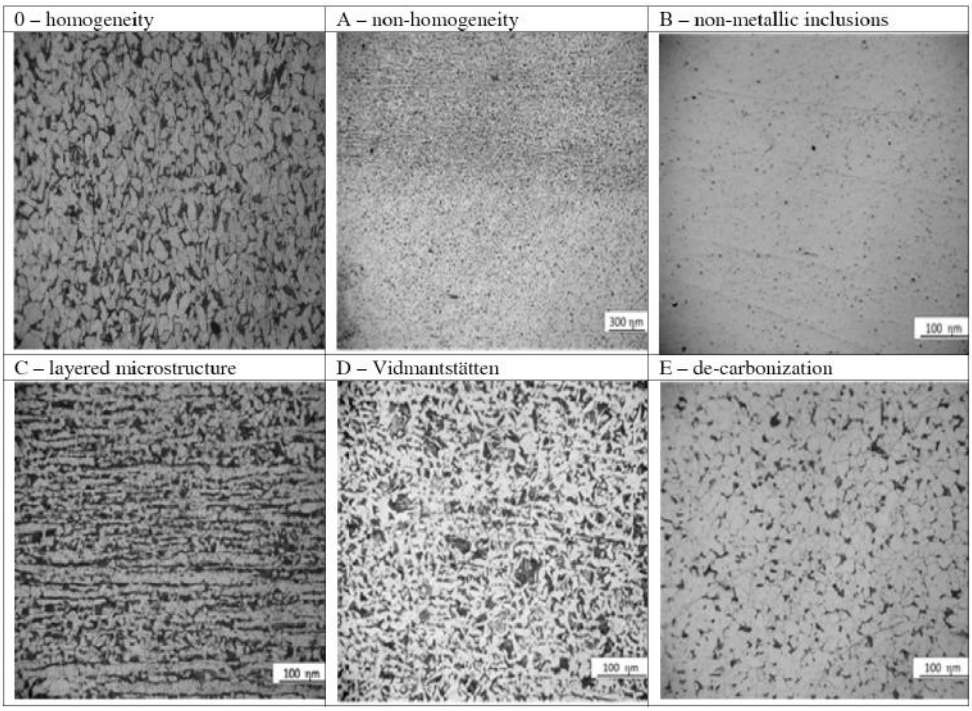

Fig. 5. Different microstructure patterns in the profiles made of St3 steel.

To substantiate deviations of mechanical properties the microstructural analysis was used as additional unquestionable tool explaining how several specimens may deform like. All samples have mechanical properties similar to St3 steel (GOST 380-88). For many studied samples the microstructural inhomogeneity takes place and one can be found in some areas with lower/higher content of carbon of around 0.1 and 0.3%, respectively. The samples with more homogenous microstructural areas contain 0.14–0.22% of carbon. The microstructural heterogeneity is usually inherited during crystallization in steel ingot, in which the amount of carbon concentrates on the ingot edges, in contrast to its center.

The amount of carbon in different areas of microstructure is different. Typically, to remove such chemical heterogeneity an annealing is used, but it is expensive and time-consuming, and it is usually applied for high-quality steel.

2. **Theoretical Details**. For elastic-plastic materials, only unique incremental relationship between stress and strain increments can be written and expressed in terms of the stress and deformation history [4]. This is illustrated in Fig. 6.

In Fig. 6, the strain increment $d\varepsilon$ is decomposed into two parts: the elastic strain increment $d\varepsilon_e$ and the plastic strain $d\varepsilon_p$. The general incremental relationship can then be written as

$$d\varepsilon = d\varepsilon_e + d\varepsilon_p \tag{1}$$

and

$$d\sigma = E_t d\varepsilon = E d\varepsilon_e = E_p d\varepsilon_p, \tag{2}$$

where $d\sigma$ is the corresponding stress increment, and E, E_t, and E_p moduli are functions of deformation history.

For a given deformation history, they may be derived from an experimental stress–strain curve under monotonic loading condition with an assumed hardening rule.

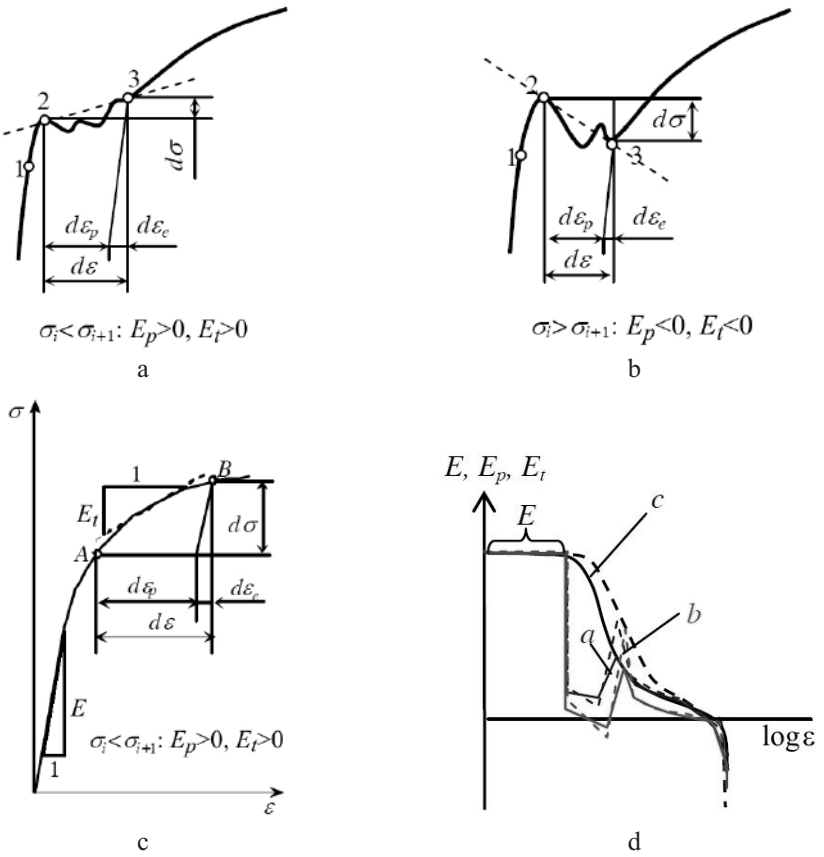

Fig. 6. Models of stress and strain history: (a) increasing yielding points; (b) decreasing yielding points; (c) tensile diagram without yielding; (d) change in moduli E, E_t, and E_p for cases (a), (b), and (c), respectively.

Note that

$$E_t = \frac{d\sigma}{d\varepsilon} = \frac{d\sigma}{d\varepsilon_e + d\varepsilon_p}, \qquad E_p = \frac{d\sigma}{d\varepsilon_p}, \tag{3}$$

from which we obtain the relation

$$\frac{1}{E_t} = \frac{1}{E} + \frac{1}{E_p}, \tag{4}$$

or

$$E_t = \frac{EE_p}{E + E_p}, \qquad E_p = \frac{EE_t}{E - E_t}. \tag{5}$$

The increments of moduli E_{ti} and E_{pi} by the change of general strain ε_i are given. Using Eqs. (3) and (4) we have the dependences between the moduli E_{ti} and E_{pi} and experimental strains ε_{ei} and ε_{pi}. Then dividing E_{ti} by E_{pi}

$$\frac{E_{ti}}{E} = 1 - \frac{\varepsilon_{pi}}{\varepsilon_{ei} + \varepsilon_{pi}} \qquad \text{and} \qquad \frac{E_{pi}}{E} = \frac{\varepsilon_{ei} + \varepsilon_{pi}}{\varepsilon_{pi}} - 1 = \frac{\varepsilon_{ei}}{\varepsilon_{pi}}. \tag{6}$$

For a given stress increment, the loading state firstly should be checked. In the case of plastic loading, the plastic strain accumulates. For a given strain increment constituting a plastic loading, we have

$$d\varepsilon_p = \frac{d\sigma}{E_p}, \tag{7}$$

$$\sigma_{t,p} = (E_{t,p})_i \int_i^{i+1} (d\varepsilon_{t,p})_i, \tag{8}$$

where $i = 1, \ldots, n$ is a number of integrating steps.

In all cases, it was observed that $|E|_t < |E|_p$ (Fig. 7). As an exception is their values on the line EPL where these quantities are equal $|E|_t = |E|_p$ because in some range if $|d\sigma| \to 0$, tangential and plastic strains increase up to $d\varepsilon_t \to \infty$, $d\varepsilon_p \to \infty$, while elastic strains are $d\varepsilon_{ei} \to 0$. This situation may happen if deformational curve passes trough the line of elastic-plastic limit (EPL), that is, goes down from the range of elasticity and plasticity (R-EP) to the range of pure plasticity (R-PP). It also should be said that in the R-PP both tangent and plastic module become negative $E_t < 0$ and $E_p < 0$, respectively. It has been obviously shown that over said negative module appear in the ranges of yielding (specimens Nos. 1, 7, and 8) and necking (specimens Nos. 1–8).

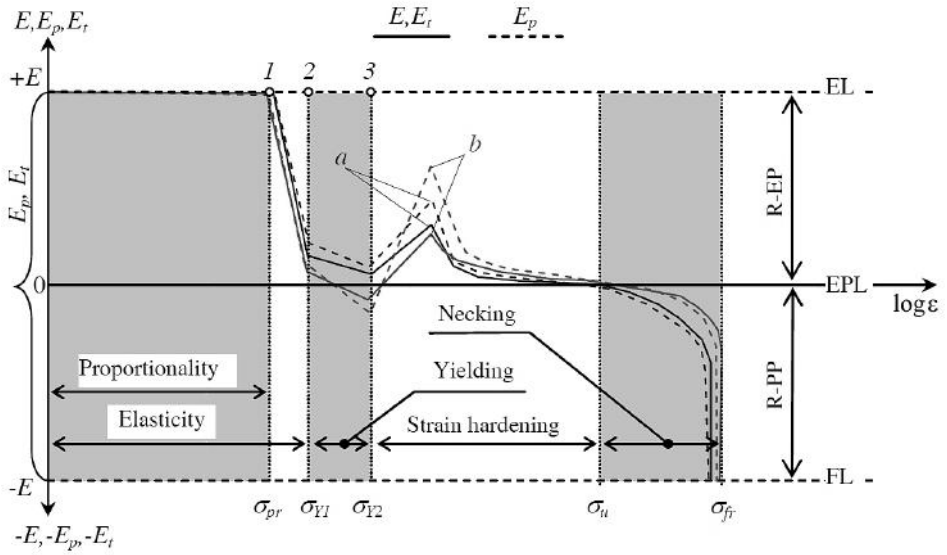

Fig. 7. Graphical exclusion of elastic and plastic behavior of St3 steel using Eqs. (1)–(8): *a* is specimen with $E_t > 0$, $E_p > 0$ (specimens Nos. 2–6) and *b* is $E_t < 0$, $E_p < 0$ (specimens Nos. 1, 7, and 8). Explanation of abbreviations: R-EP – range elastic-plastic; R-PP – range of perfect plasticity; EPL – elastic-plastic limit; FL – fracture limit; EL – elasticity limit.

The generalizations shown in range $\sigma_{Y1} - \sigma_{Y2}$ overcome all the picks of yielding and ones have not been evaluated individually trying to explain full curvature but rather this range has been used to join Points *2* and *3* showing a general tendency and angle of yielding with $E_t > 0$, $E_p > 0$ or $E_t < 0$, $E_p < 0$ (Fig. 6a, b). The yielding "picks" and "wells" are the result of superposed impact and relaxation of microprocesses occurring in different places of specimen due to tension. Point *3* shows the end of yielding beyond which values E_t and E_p start growing up because of the change in the curve angle, as compared to the range of points *2–3* (Figs. 6 and 7).

3. **Results**. The results obtained are listed in Table 4 and depicted in Fig. 8. Despite the randomness of processes and a large number of sets that present possible relations between the microstructural feature, its level and deformational behavior, of the most concern is the history of deformation in terms of tangent and plastic moduli E_t and E_p, respectively. Taking all the microstructural features and their levels into account it is difficult to decide which feature dominates as the main influence on the mechanical properties especially if there are levels not well expressed, say levels I and II (specimens Nos. 4 and 7) or they are similarly high levels IV and V (specimens Nos. 1 and 5).

T a b l e 4

Mechanical Properties and Steps of Stress Ranges Used in Determination of Moduli E, E_{ti}, and E_{pi}

Mechanical characteristic	Specimen number							
	1	2	3	4	5	6	7	8
ε_e	0.1410	0.1380	0.1593	0.1413	0.1489	0.1401	0.1420	0.1876
σ_e	284.15	286.72	332.69	282.85	286.80	282.84	282.61	289.23
ε_{Y1}	0.2350	0.6690	0.4276	0.4236	0.5389	0.2520	0.4969	0.3137
σ_{Y1}	290.56	312.52	345.59	296.53	290.29	285.97	301.09	293.73
ε_{Y2}	1.0190	1.2730	1.2770	1.2930	1.2750	0.9210	1.2560	0.9645
σ_{Y2}	280.59	322.46	362.63	311.83	303.43	288.90	298.56	288.67
ε_u	8.8140	8.6520	8.4900	8.9300	9.4300	8.7750	10.0700	9.8255
σ_u	394.63	448.49	509.33	436.79	414.49	399.03	430.04	422.35
ε_{fr}	11.1530	10.9370	12.8350	13.1600	12.3840	10.7930	13.0970	12.5700
σ_{fr}	326.91	376.20	398.62	346.37	340.18	338.20	344.08	378.36
$d\sigma_{Y-u}$ (> 0)	11.40	12.60	14.67	12.50	11.11	11.01	13.15	13.37
$d\sigma_{u-fr}$ (< 0)	−11.30	−10.33	−11.07	−11.30	−13.14	−10.14	−10.75	−11.00

In the range of stress $d\sigma$, the signs $+/-$ representing moduli E, E_t, and E_p may be gotten as follows:

$$\begin{cases} E = \text{const}, \\ [0,\ \sigma_e]\text{: } E_t = E \text{ and } E_p = E, \\ [\sigma_Y,\ \sigma_{Y1}]\text{: } E_t > 0,\ E_p > 0 \text{ and } E > E_p > E_t, \text{ if } \sigma_{i+1} - \sigma_i > 0, \\ \text{or } [\sigma_Y,\ \sigma_{Y1}]\text{: } E_t < 0,\ E_p < 0 \text{ and } E > E_t > E_p, \text{ if } \sigma_{i+1} - \sigma_i < 0, \\ [\sigma_{Y1},\ \sigma_u]\text{: } E_t > 0,\ E_p > 0 \text{ and } E > E_p > E_t, \text{ if } \sigma_{i+1} - \sigma_i > 0, \\ [\sigma_u, \sigma_{fr}]\text{: } E_t < 0,\ E_p < 0 \text{ and } |E_t| \approx |E_p| \Rightarrow |E|, \text{ if } \sigma_{i+1} - \sigma_i < 0. \end{cases} \tag{9}$$

Noteworthy is the reached stressed state, strain range, and the material strain limit. To analyze the strength of pole structural elements made of St3 steel, we evaluated the material mechanical properties influenced by two factors: 1) external damages caused by corrosion; 2) a microstructural variety influenced by differences in thermal gradient related to dimensions of pole elements.

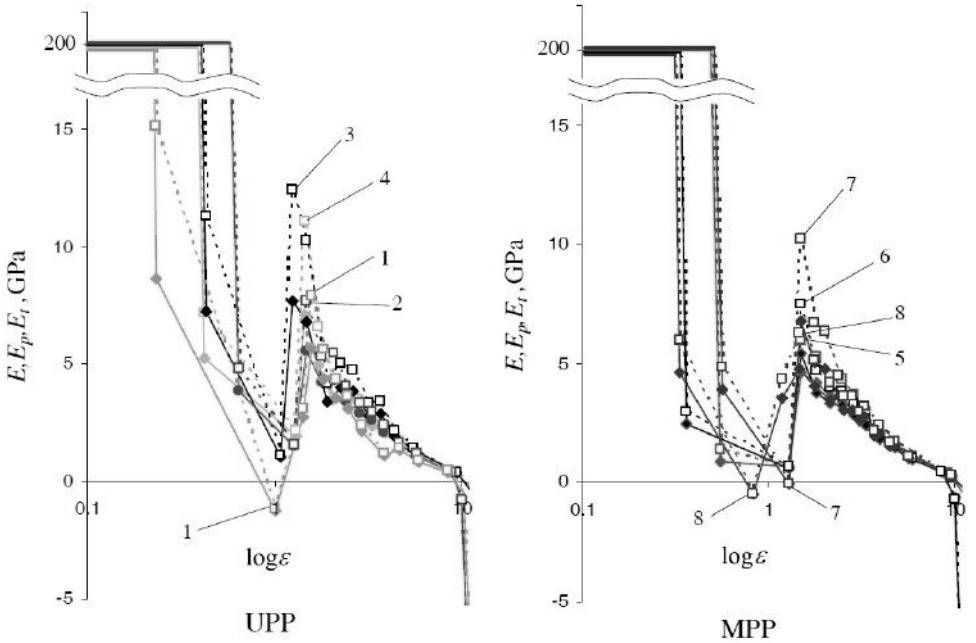

Fig. 8. Graphical exclusion of elastic and plastic behavior in terms of moduli E, E_{ti} (solid), and E_{pi} (dashed).

When the engineering stress values were calculated and compared, it was stated that the corrosion depth had no influence on the yield, ultimate, and fracture stresses, when the average of total (on both specimen sides) corrosion depths was in the range from 0.1 to 0.25 mm. According to the outer character of corrosion seen on a surface of angle, the clear tendencies influencing on the well expressed mechanical properties were not found (Fig. 9). As the exception of over said result it was taken mechanical properties of specimens No. 3 representing minimal value of corrosion depth. In addition, the corrosion depth may cooperate with some so called "unstable" microstructures.

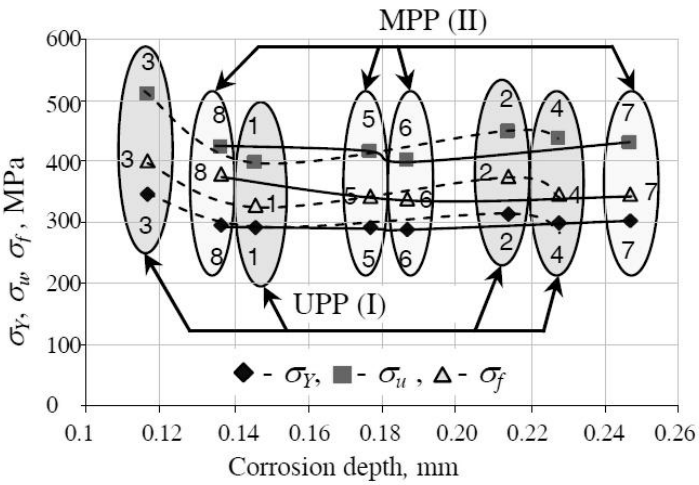

Fig. 9. Engineering mechanical properties versus corrosion depth at fracture area. UPP (I): specimens Nos. 1–4 (dashed); MPP (II): specimens Nos. 5–8 (solid).

T a b l e 5

True Strains e, Stresses S, and Relative Reduction of Cross Section ψ

Mechanical characteristic	Units	Specimen number							
		1	2	3	4	5	6	7	8
e_u	Arbitrary m.u.	0.328	0.368	0.231	0.355	0.295	0.396	0.259	0.306
e_f		0.769	0.725	0.70	0.753	0.706	0.729	0.620	0.658
Δe_{f-u}		0.441	0.357	0.469	0.398	0.411	0.333	0.361	0.352
S_u	MPa	710.9	671.1	673.0	697.2	603.5	752.2	724.6	638.2
S_f		556.9	560.5	526.5	582.0	517.0	639.2	643.2	579.4
ΔS_{f-u}		154.0	111.1	146.5	115.2	86.5	112.9	81.4	58.8
ψ	%	50.57	52.28	46.23	48.18	51.51	51.09	50.35	52.9

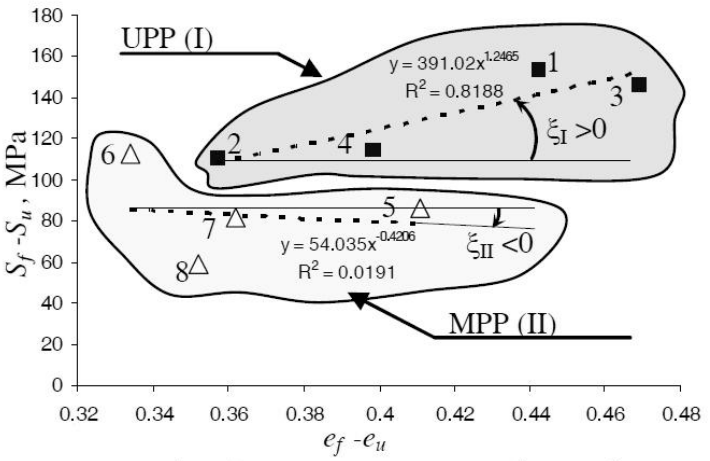

Fig. 10. Graphical representation of the exclusion of differences in the mechanical characteristics for UPP (I) (specimens Nos. 1–4) and MPP (II) (specimens Nos. 5–8) as $\Delta S_{f-u} = f(\Delta e_{f-u})$.

The second (microstructural) point of view has revealed clear dissimilarities that were picked out in two separate sets in terms of differences $\Delta S_{f-u} = S_f - S_u$ and $\Delta e_{f-u} = e_f - e_u$ by a function $\Delta S_{f-u} = f(\Delta e_{f-u})$ presented in Fig. 10. The symbols S and e represent the true stresses and true strains at the fracture and ultimate points, respectively. The standard equations on true stresses and strains were used: ultimate and fracture stresses are $S_u = F_u / A_u$ and $S_f = F_f / A_f$, respectively; ultimate and fracture strains are $e_u = \ln(1+\varepsilon_u)$ and $e_f = \ln(1+\varepsilon_f)$. As the comparative characteristic of plasticity the relative reduction of cross section ψ was taken into account – $\psi = \dfrac{A_1 - A_0}{A_0} \times 100\%$. One was used for a deformability assessment beyond the point of ultimate stress trying to achieve results showing a tendency the material more elongates by Δe_{f-u} or contracts by ψ. Calculation results are shown in Table 5.

As seen in Fig. 10, two specimen groups are located in the two different sets UPP (I) and MPP (II), respectively. Using an approximation by power function X^{α}, the resulting graphical data are aligned by different angles ξ_{I} and ξ_{II} called deformational sensitivity parameters (DSP). The power function then is

$$Y_{\mathrm{I,II}} = (CX^{\alpha})_{\mathrm{I,II}}. \tag{10}$$

Using mechanical characteristics from the graph of Fig. 10, Eq. (10) may be rewritten as

$$(\Delta S_{f-u})_{\mathrm{I,II}} = \{C(\Delta e_{f-u})^{\alpha}\}_{\mathrm{I,II}}, \tag{11}$$

where coefficients C and α are as follows: $C_{\mathrm{I}} = 391.02$, $\alpha_{\mathrm{I}} = 1.2465$ for the UPP (I) and $C_{\mathrm{II}} = 54.035$, $\alpha_{\mathrm{II}} = 0.4206$ for the MPP (II). These coefficients approximate a rate in differently distributed ranges of true stresses $S_f - S_u$ and strains $e_f - e_u$.

The deformational sensitivity parameters ξ_{I} and ξ_{II} take the relation of the ranges ΔX on axis x and the range ΔY on axis y as

$$\xi_{\mathrm{I,II}} = \frac{(Y_2 - Y_1)_{\mathrm{I,II}}}{(X_2 - X_1)_{\mathrm{I,II}}} = \left(\frac{\Delta Y}{\Delta X}\right)_{\mathrm{I,II}}. \tag{12}$$

Using the comparison ξ_{I} and ξ_{II} we obtained values of a relative deformational sensitivity parameter (RDSP) that quantatively showed two different qualities in the microstructures of UPP (I) and MPP (II). The RDSP was designated as $\bar{\xi}$, and it is equal to

$$\bar{\xi} = 1 - \frac{\xi_{\mathrm{II}}}{\xi_{\mathrm{I}}}. \tag{13}$$

Using Eqs. (10)–(13) were obtained following results. For the upper pole part: $(X_1)_{\mathrm{I}} = 0.36$, $(X_2)_{\mathrm{I}} = 0.46$, $(Y_1)_{\mathrm{I}} = 109.428$ MPa, $(Y_2)_{\mathrm{I}} = 148.534$ MPa, $(\Delta X)_{\mathrm{I}} = 0.1$, $(\Delta Y)_{\mathrm{I}} = 39.106$, and $\xi_{\mathrm{I}} = 391.06$ MPa; for the upper pole part: $(X_1)_{\mathrm{II}} = 0.34$, $(X_2)_{\mathrm{II}} = 0.4$, $(Y_1)_{\mathrm{II}} = 85.062$ MPa, $(Y_2)_{\mathrm{II}} = 79.442$ MPa, $(\Delta X)_{\mathrm{II}} = 0.06$, $(\Delta Y)_{\mathrm{II}} = -5.62$ MPa, and $\xi_{\mathrm{II}} = -93.667$ MPa; and $\bar{\xi} = 1.24$.

Summing up the results it should be noted that the corrosion depth measured in the range from 0.1 to 0.25 mm had no significant influence on the stress and strain values. This is the main difference between earlier formulated deformability restrictions and the RDSP criterion based on parameter $\bar{\xi}$ expressing the microstructural variety of St3 steel.

4. **Discussion**. The upper part of the pole was tested using specimens Nos. 1, 2, 3, and 4. The tensile test results of Specimen 1 show mechanical properties distributed between specimens Nos. 2 and 3. It is obvious because of inhomogeneity (A, IV) that is visible closer to the surface of the specimen as partially decarbonized (E, I) microstructure while remaining volume is homogeneous (0) enough. The worst results were observed in specimen No. 2. In its microstructure, the visible inhomogeneity is related with a large amount of nonmetallic inclusions. The layered microstructure (C, II) is a bit less expressed in comparison with other specimens, so it should not influence on the drastic changes in strength and plasticity. Also, the volumes with nonmetallic inclusions (B, V) are less than in specimen No. 3. However, specimen No. 3 layered microstructure is very strongly expressed (C, III). In specimen No. 2, Widmanstätten microstructure (D, II) was observed, too. These kinds of defects were formed in the areas of large grains of pearlite with like-needle ferrite inserts inside. Such a defect occurs during thermal impact by high temperature. It happens especially in those cases if alloy is retained long enough and cooled a bit too quickly. Widmanstätten usually negatively influences on the mechanical properties of the St3 steel. Other feature like layered microstructure is not completely negative to be considered as a serious microstructural defect when ferrite and pearlite grains are distributed

separately in paths and form so called layered microstructure. In the case of tensile loads applied parallel to the layered microstructure we usually observe better mechanical properties (specimen No. 3, C, III). Specimen No. 3 represents the best results. Its microstructure is homogeneous (0) with small amount of nonmetallic inclusions (B, I), however, the layered microstructure (C, III) has higher level than it was in specimen No. 2 (C, II).

The middle part of the pole was tested using specimens with Nos. 5, 6, 7, and 8. Comparing the results of mechanical properties of specimens Nos. 5 and 6, it may be said that the main factors influencing on the strength characteristics are nonmetallic inclusions (B) and layered microstructure (C). More plastic sulfides are common and ones can be observed in several specimens, but their negative effect is usually manifested in such cases if they are located in the transverse direction to the load. In rolled structural elements, these inclusions are parallel to the rolling direction. Specimen No. 5 has higher level of Widmanstätten (D, II). Inhomogeneity (A, IV) was obviously stronger in specimen No. 5 and this was determinant factor because Widmanstätten in specimen No. 6 was not so strong (D, I). For specimens Nos. 7 and 8, the main factors describing differences in mechanical properties are nonmetallic inclusions (A) and layered microstructure (C). In these specimens the amount of nonmetallic inclusions (B, I) is less that is why the impact to yield stress σ_Y and ultimate stress σ_u becomes increasing. The amount of layered microstructure is also expressed a little (C, II) and positively influences on the high position of points for stresses σ_Y and σ_u. Specimens Nos. 7 and 8 have approximately same values σ_Y and σ_u but relative elongation δ is greater in specimen No. 7. The features influencing this phenomenon may attributed to the low level of inhomogeneity (A, II). A high level of nonmetallic inclusions (B, V) is presumably responsible for small values of δ in specimen No. 6.

It should be mentioned that layered microstructure (C) forms a bit far away from rolled surface in range A1–A3 and concentrates in the middle part of cross section along to direction of rolling. This happens because of additional heating and an extension of cooling time when rolled sheet comes in the contact with rolling wheels. In other words, additional heat is influenced by deformational process. Since external layers are deformed more then microstructure goes without like-layers paths in which an annealing takes place. The deeper allocation of layered microstructure (C) is led by more deformation. A like-fiber layered microstructure (C) consists of much harder/stronger part together with mild/plastic part. A sulfides' influence on the mechanical properties is small enough because they are distributed longitudinally to the rolling direction. In the case of oxides' fireplaces, a large amount of ones can easily connect with each other and give a start to a material weakening. Oxides especially are dangerous if they are concentrated in one area with large amount and high density, in comparison with randomly distributed and less dense areas.

Conclusions. The performed analysis shows that there is a weak statistical relation between the corrosion depth, area damaging the surface of examined specimens and the mechanical properties due to quasistatic loading conditions. The microstructural phenomena might be strongly influenced by the casting of alloy used for elements production of high voltage poles. Sometimes, it can cause also the corrosion areas and depths on the outer specimen surface. Other external factors related to air quality also would be taken into account if corrosion influence on mechanical properties were high enough. The human factor as negative feature can be excluded because the distribution of corrosion sources is approximately the same in all pole parts, which means that covering technology of surfaces satisfies technological requirements of that time.

As a general conclusion, it can be said that the main factors affecting the mechanical properties of all reviewed specimens are nonmetallic inclusions, layered microstructure and low homogeneity of St3 steel. All these material quality related factors were quantatively filtered by the calculating of relative deformational sensitivity parameter (RDSP). It has

shown that the differences in microstructure deteriorate the mechanical properties by 24% ($\bar{\xi} = 1.24$). The results depicted in Figs. 5 and 10 and calculated via Eqs. (10)–(13) strongly indicate that the profile microstructure cut from the upper pole part (I) is less homogeneous than that cut from the middle pole part (II), which is instrumental in practical applications.

Р е з ю м е

Установлены причины изменения механических свойств холоднокатаных уголков, изготовленных из низкоуглеродистой стали Ст3, для старых конструкций высоковольтных опор. Изучен ряд кинетических кривых, описывающих механические свойства, в виде касательных и пластических модулей как наиболее приемлемых характеристик, поскольку обобщенные параметры могут более четко отражать изменения прочности и деформируемости на любом этапе деформирования. Представлены исходные количественные характеристики с целью исключения влияния качества элементов опор при их изготовлении, чтобы показать значение деформационного поведения для объяснения микроструктурного разнообразия. Микроструктурные характеристики могут оказывать влияние на уровень напряжений в точках текучести, предела прочности и разрушения.

1. P. Baltrünas, D. Butkus, V. Oškinis, et al., *The Environment Saving* [in Lithuanian], Technika, Vilnius (2008).
2. H. Karagah, C. Shi, M. Dawood, and A. Belarbi, “Experimental investigation of short steel columns with localized corrosion,” *Thin Wall. Struct.*, **87**, 191–199 (2015).
3. L.-V. Beaulieu, F. Legeron, and S. Langlois, “Compression strength of corroded steel angle members,” *J. Constr. Steel Res.*, **66**, No. 11, 1366–1373 (2010).
4. W. F. Chen and H. Zhang, *Structural Plasticity: Theory, Problems, and CAE Software*, Springer-Verlag, New York (1991).

Received 20. 07. 2017